https://doi.org/10.5194/egusphere-2022-1214
Preprint. Discussion started: 9 January 2023

Implications of the tectonic rotation of the South Qiangtang Massif for the subduction closure of the BangongCo - Nujiang Tethys Ocean - A study of magnetic fabric and zircon U-Pb chronology

Qinglong Chen[1], Xin Cheng[1], Feifei Huo[1,b], Yanan Zhou[1], Nan Jiang[1,c], Bitian Wei[1], Baofeng Wang[1,d], Pengxiang Xu[1,d], Dongmeng Zhang[1], Longyun Xing[1], Teng Li[1], Feifan Liu[1], Jingyue Wu[1], Jiawei Wang[1], Hanning Wu[1*], and the Northwest University Paleomagnetism Team+

[1] State Key Laboratory of Continental Dynamics, Department of Geology, Northwest University, Xi'an, 710069, China
[b]now at: College of Engineering, Zunyi Normal University, Zunyi Guizhou 563006, China
[c]now at: College of Petrol and Environment Engineering, Yan'an University, Yan'an 716000, Shaanxi, China
[d]now at: Gansu Provincial Coal Geological Exploration Institute, Lanzhou 730000, China
+A full list of authors appears at the end of the paper.

Correspondence: Qinglong Chen; chenqinglong@stumail.nwu.edu.cn
Hanning Wu; wuhn2506@nwu.edu.cn

Abstract: In the BangongCo-Nujiang Tethys Ocean, the timing of closure and subduction polarity are key issues in the study of the Tethys domain. Detailed magnetic fabrics and zircon U-Pb dating of marine carbonates collected in the South Qiangtang Massif and clastic rocks collected in the Ban-Nu Suture Zone were carried out to constrain their subduction and collapse processes, from the Middle to Late Jurassic-Early Cretaceous. The results show that the Shamuluo Formation in the suture zone is 131-95 Ma in age, which belongs to the Late Jurassic-Early Cretaceous and develops a primitive sedimentary magnetic fabric; Under the tectonic stress, the limestones in the Middle Jurassic Buqu Formation developed the strongly cleaved magnetic fabric. Meanwhile. the sandstones in the Late Jurassic Sowa Formation developed the tensile lineation and initial deformaed magnetic fabrics. Integrated magnetic fabrics, zircon U-Pb chronology and petrographic studies suggest a WE to SW-NE anticlockwise sinistral movement in the South Qiangtang Massif from the Buqu Formation to the early Suowa Formation; In the Late Suowa Formation, it began a clockwise dextral movement. The change in the direction of massif rotation was associated with a change in the subduction polarity of the BangongCo-Nujiang Tethys Ocean. The BangongCo-Nujiang Ocean changed from southward subduction to northward subduction, which began at the Buqu Formation and ended at the late Sowa Formation (163.5-157.3 Ma).

https://doi.org/10.5194/egusphere-2022-1214
Preprint. Discussion started: 9 January 2023

Afterwards, it began to close at 145 Ma and ended its subduction after 131-109.9 Ma, achieving complete closure of the central BangongCo - Nujiang Tethys Ocean.

Key words: BangongCo-Nujiang Tethys Ocean; South Qiangtang Massif; closure time; subduction polarity; magnetic fabric; zircon U-Pb chronology

0 Introduction

Most rocks contain ferromagnetic minerals, and tectonics causes deformation or dynamic recrystallisation of them, resulting in their directional alignment, causing the anisotropy of magnetic susceptibility (Lu et al, 2008). The magnetic record of tectonic action through mineral deformation is expressed as magnetic fabric. Because of the good correspondence between rock magnetization ellipsoids and strain ellipsoids (Kneen, 1976; Rathore, 1979), they are widely used for tectonic deformation, paleostress recovery (Borradaile and Henry, 1997), and sediment palaeoflow (Gurioli et al, 2005), etc. Thus, it is possible to analyze the tectonic deformation, as well as the manner and direction of stress action. In addition, combining zircon U-Pb chronology with magnetic fabric allows greater constraints on tectonic evolutionary processes.

The subduction and closure of the BangongCo-Nujiang Tethys Ocean is an important tectonic event of the formation and evolution in the Tibetan Plateau (Yin and Harrison, 2000; Metcalfe, 2013). Existing studies generally agree that the onset of subduction for the BangongCo-Nujiang Tethys Ocean occurred from the Early-Middle Jurassic to Early Cretaceous (Yin and Harrison, 2000; Guynn et al, 2006; Kapp et al, 2007; Zhu et al, 2016), but there is considerable disagreement about the exact timing. To start with, intercalated bioclastic rocks mixed in the OIB basalt (120-108 Ma) of the Ban-Nu Suture Zone, supports the onset of subduction in the Middle Jurassic (Liu et al, 2014); Furthermore, deep geophysics and mantle dynamics consider that the Ban-Nu Ocean was subducted under the Qiangtang Massif at 110 Ma (Kapp et al, 2007); Moreover, zircon chronology of collisional granites explains that the Ban-Nu Ocean was still subducted at 120-110 Ma (Li et al, 2022). As for the subduction polarity, there are three views: northward, southward. North-south bi-directional suduction. (1) Early Jurassic MORB-type (-180 Ma), arc-front ophiolites (Gyunn et al, 2006; Wang et al, 2016) in SSZ-type (190-180 Ma) and high-Mg andesites represent an arc-trench system of northward subduction in the Tethys Ocean (Whattam and Stern ,2011; Ishizuka et al, 2014); (2) Extensive outcrops of the MugaGangri mélange correspond to a southward subduction of the pre-arc basin; (3) The high and low calcium-alkaline content basalts separated from the volcanic rocks of the North Lhasa Massif suggest plate reversal and plate breakage (Gvirtzman and Nur, 1999; Grove et al, 2009). Furthermore, the Ban-Nu Ocean was subducted north-south (116-100 Ma) in both directions in response to mantle flow circulation.

Therefore, it is crucial to clarify the timing of closure and the subduction polarity of the BangongCo-Nujiang Tethys Ocean. While this paper is proposed to combine magnetic fabrics analysis with zircon U-Pb dating studies. Petrological, magnetic fabric and zircon chronological studies were carried out on the Buqu and Suowa Formations of the Middle-Late Jurassic in the South Qiangtang Massif, as well as, the Shamuluo Formation of the Late Jurassic-Early Cretaceous in the Ban-Nu Suture Zone. The studies will limit the closure time and constrain their subduction process of the BangongCo-Nujiang Tethys Ocean, from the Middle-Late Jurassic to Early Cretaceous.

1 Geological background

The BangongCo-Nujiang Suture Zone is located in the central Tibetan Plateau, dividing the Qiangtang Massif to the north and the Lhasa Massif to the south, which represents the vanishing BangongCo-Nujiang Tethys Ocean (Yin and Harrison, 2000; Pan et al, 2012). The evolution of the Ban-Nu Suture Zone is complex, including successive outcrops of Jurassic ophiolite, subduction accretionary detrital rocks and medium acidic magmatic rocks (Figure 1(a)). The suture zone and the extensively developed magmatic rocks on both sides record geological information on the subduction closure, plate breakup and crustal dismantling of the Ban-Nu Ocean (Zhu et al, 2011,2016; Hu et al, 2017). While to its north, from the Jurassic to Early Cretaceous period, the South Qiangtang Massif developed a foreland basin under the effect of ocean-land collision. As for the foreland basin, it appears an uncomfortable contact with the underlying strata and a sand-mudstone complex marble deposit, showing an early wedge-shaped sedimentary body of the foreland basin. This gradual change from Middle Jurassic-Late Cretaceous to marine molasse deposits marks a transform in the nature of deposition in the South Qiangtang Massif.

Under the subduction background, the Shamulo Formation clastic rocks exposed in the BangongCo-Nujiang Suture Zone are active continental margin deposits with residual sea basin properties in the Ban-Nu Ocean, from the Middle-Late Jurassic to Early Cretaceous (Wu et al, 2021). As for its lithological composition comprises a suite of shallow metamorphic slates, sandstones interbedded with carbonates, andesites and andesitic crystalline tuffs. Besides, the Shamuluo Formation is in angularly unconformable contact with the Lower MugaGangri Group.

The Buqu and Suowa Formations in the Middle-Late Jurassic belong to the South Qiangtang Massif, which is a sea-land transitional phase of shallow water-land shelf deposits, developing carbonates and clastic rocks. The lithological composition of the Buqu Formation was made up of thickly bedded bioclastic tuffs, micrite interbedded with bioclastic tuffs and dolomitic micrite, distinguished from the Tuotuohe Formation by grey-black bioclastic tuffs at the base. The lower section of the Suowa Formation develops red-grey marl and bioclastic micrite, whose upper section develops muddy siltstones (Figure 1(b)). The marl and bioclastic tuffs are developed in unequal thickness interbedded with thinly interbedded mesoscopic tuffs. Meanwhile, the sandstones develop parallel bedding and ripple marks, and the siltstone contains sporopollen and dinoflagellate fossils. Besides, the basement of Buqu Formation is in conformable contact with the Xiali Formation.

https://doi.org/10.5194/egusphere-2022-1214
Preprint. Discussion started: 9 January 2023

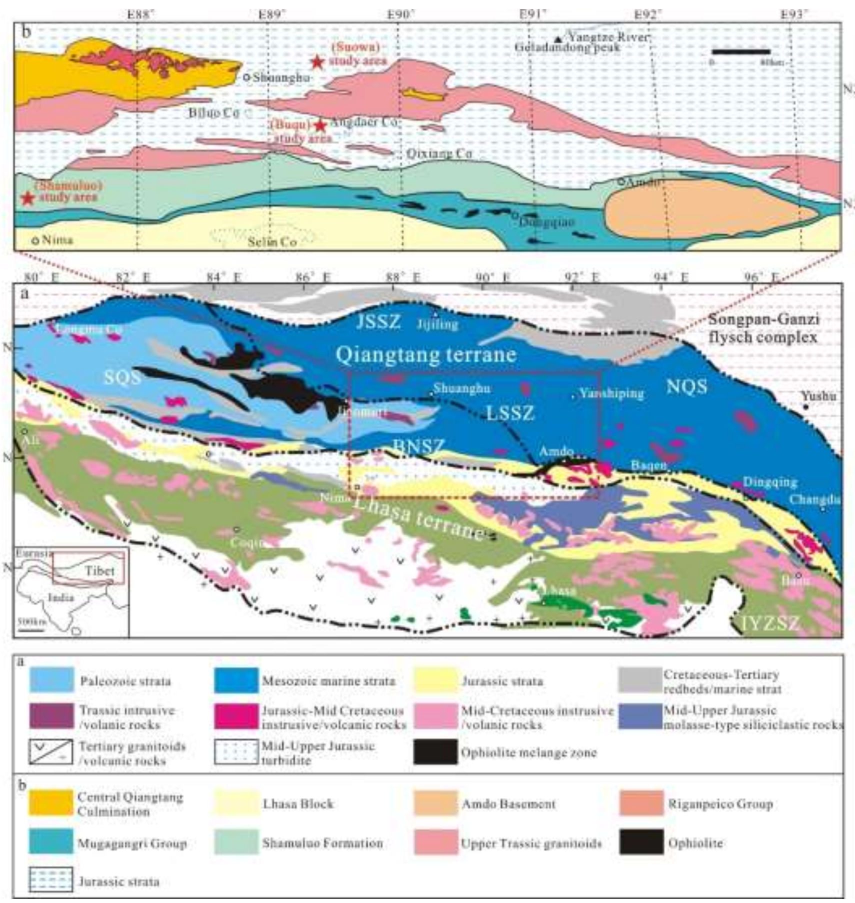

Figure 1. Sedimentary stratigraphy, lithological distribution and tectonic unit delineation in the South Qiangtang Massif and the Ban-Nu Suture Zone. (a) Geological map of the Tibetan Plateau; (b) Geological map of the study area.

2 Sample collection and testing

2.1 Sample collection

Sample collection was carried out in relevant sections in the Nyima area of the Lhasa Massif and the Shuanghu area of the South Qiangtang Massif (Figure 1(b)). Samples of the Shamuluo Formation were collected from a continuous section in the Ban-Nu Suture Zone at 32°02’02” N, 87°04’07” E. Among them, the lithology is mainly siltstone, muddy siltstone (site no. JS01-04) and volcanic clastic (site no. JS05). As for the Suowa Formation samples were collected from two sections in the South Qiangtang Massif at 33°08’07” N and 89°00’43” E, respectively. Among them, the lithology is silty mudstone and muddy siltstone (site no. J3A). In addition, samples from the Buqu Formation were collected in three profiles completed at the following

https://doi.org/10.5194/egusphere-2022-1214
Preprint. Discussion started: 9 January 2023

locations: 32°44’27” N, 89°22’37” E; 32°42’33” N, 89°22’10” E and 32°39’41” N, 89°33’19” E. Among them, the lithology is bioclastic tuff and micrite (site no. J2B), with 198 pieces collected. Beyond that, 34 sandstones and 36 volcanic clasts samples from the Shamuluo Formation and 69 sandstone samples from the Suowa Formation were collected. All samples were drilled in the field using a portable petrol drill rig, oriented and sampled using an orienteer and magnetic compass, then cut indoors into standard cylindrical samples in 2.2cm high, with the remaining samples used for rock magnetic analysis and zircon U-Pb dating.

2.2 Analysis methods

Testing and analysis of the magnetic fabric samples was completed at the State Key Laboratory of Continental Dynamics, Northwest University. The magnetic fabric analysis was carried out using a Kappabridge magnetization meter (MFK1-FB, test field strength 300 A/m, detection limit 2 x 10^{-8} SI, test accuracy 1%) from AGICO, Czech Republic, to test the anisotropy of the magnetization at low fields with room temperature (298 K, operating frequency 975 HZ), and the results were processed using Anisoft 4.2 software, while were shown in Table 1. Rock magnetics experiments include variation of magnetization with temperature (K-T) and saturated isothermal remanent magnetization (SIRM). For one thing, the magnetization variation with temperature experiments were carried out on a MFK1-FA Kappabridge multi-frequency magnetization meter, where the sample was heated from room temperature to 700°C, then gradually being cooled to room temperature. Throughout the process, the magnetization versus temperature curves obtained were used to determine the main magnetically loaded minerals in the samples. For another, the isothermal remanent magnetization (IRM) test determines the type of magnetic mineral in a sample by the variation in the magnetization and demagnetization curves. Later, the addition of the field is done using the ASC IM-10-30 pulsed magnetometer and the measurement is done using the JR-6A two-speed rotating magnetometer.

Zircon U-Pb dating tests were completed at Nanjing Hongchuang Geological Exploration Technology Service Co. Zircons with clear ring bands and intact crystal structure, without fractures and inclusions, were selected for testing. Data processing included selection of samples and blank signals, correction for instrument sensitivity drift, elemental content and U-Th-Pb isotope ratios and age calculations. And the international standard zircon 91500 and Australian zircon GJ-1 were used as external standards for isotopic correction in the U-Pb isotope dating. For U-Th-Pb isotope ratio drift related to the analysis time, a linear interpolation was used to correct for the change in 91500 (Liu et al, 2010).

Table 1. Magnetic fabric parameters of samples from the Ban-Nu Suture Zone and the South Qiangtang Massif at room temperature (RT).

Sampling site	N	Km	L	F	Pj	T	K1	K2	K3
JS01	10	130×10^{-6}	1.001	1.003	1.006	0.316	268.1/6.0	359.1/8.8	144.4/79.3
JS02	13	144×10^{-6}	1.002	1.004	1.006	0.276	289.5/0.5	19.5/0.1	123.0/89.5
JS03	5	142×10^{-6}	1.001	1.003	1.004	0.274	261.7/15.9	4.9/38.6	153.9/47.1

https://doi.org/10.5194/egusphere-2022-1214
Preprint. Discussion started: 9 January 2023

JS04	6	119×10-6	1.002	1.003	1.005	0.218	199.4/4.7	290.1/8.0	79.4/80.7
Shamuluo profile (mean)	34	135×10-6	1.002	1.003	1.005	0.277	265.5/5.2	356.0/6.2	135.7/81.9
J3SA01	6	57.6×10-6	1.052	1.006	1.065	-0.238	98.0/59.3	263.4/29.9	357.1/6.4
J3SA02	7	46.2×10-6	1.009	1.004	1.014	-0.228	220.4/77.6	101.8/6.0	10.7/10.8
J3SA03	14	82.2×10-6	1.011	1.003	1.016	-0.520	351.5/78.1	213.3/8.9	122.1/7.8
Suowa profile 1(mean)	27	67.4×10-6	1.020	1.004	1.026	-0.386	88.9/77.3	274.9/12.6	184.6/1.3
J3SA01	8	35.4×10-6	1.004	1.006	1.010	0.239	293.9/45.1	201.4/2.5	109.0/44.8
J3SA02	9	34.3×10-6	1.003	1.004	1.007	0.109	204.1/0.1	294.1/37.0	114.0/53.0
J3SA03	7	34.3×10-6	1.003	1.006	1.010	0.326	354.4/15.7	254.7/30.8	107.7/54.67
J3SA04	7	31.4×10-6	1.004	1.006	1.010	0.166	171.7/2.0	262.5/20.3	76.2/69.611
J3SA05	11	29.2×10-6	1.006	1.006	1.013	-0.008	338.6/22.6	246.6/5.0	144.9/66.8
Suowa profile 2(mean)	42	32.7×10-6	1.004	1.006	1.010	0.149	341.5/21.9	242.5/21.3	112.8/58.7
J2BA01	8	15.8×10-6	1.012	1.033	1.048	0.263	331.7/29.5	240.0/3.1	28.2/18.9
J2BA02	8	11.1×10-6	1.006	1.015	1.022	0.426	325.4/5.2	235.0/4.2	106.2/83.3
J2BA03	10	21.8×10-6	1.014	1.031	1.048	0.223	33.6/20.1	289.2/34.1	148.4/48.9
J2BA04	8	18.0×10-6	1.014	1.022	1.037	0.211	26.3/20.2	271.5/48.8	130.7/34.1
J2BA05	6	31.4×10-6	1.024	1.066	1.096	0.431	24.8/29.2	283.3/19.6	164.4/53.7
J2BA06	9	15.7×10-6	1.012	1.020	1.034	0.183	41.2/20.6	292.6/40.2	151.5/42.6
J2BA07	8	11.4×10-6	1.009	1.019	1.029	0.301	235.7/29.7	143.3/4.2	46.0/60.0
J2BA08	8	475×10-6	1.009	1.025	1.036	0.424	14.9/26.2	267.2/31.8	136.3/46.6
J2BA09	8	19.1×10-6	1.010	1.045	1.059	0.592	31.3/5.2	297.7/34.6	128.8/54.9
Buqu profile 1(mean)	74	67.2×10-6	1.012	1.029	1.044	0.331	27.7/18.2	286.2/31.3	143.2/52.7
J2BB10	19	19.3×10-6	1.010	1.039	1.053	0.523	27.6/26.9	294.7/5.8	193.6/62.4
J2BB11	6	12.1×10-6	1.020	1.060	1.085	0.470	93.3/21.2	352.2/26.3	217.1/55.1
J2BB12	11	15.1×10-6	1.022	1.039	1.064	0.237	70.8/22.1	328.1/28.5	192.9/52.6
J2BB13	10	32.1×10-6	1.009	1.029	1.040	0.377	250.2/74.3	29.3/12.0	121.5/10.0
J2BB14	11	47.3×10-6	1.018	1.075	1.101	0.596	333.4/76.1	228.9/3.5	138.0/13.4
J2BB15	7	58.0×10-6	1.014	1.066	1.087	0.576	334.0/75.9	230.5/3.3	139.7/13.7
J2BB16	13	45.9×10-6	1.016	1.055	1.076	0.546	8.5/69.4	227.4/16.3	133.8/12.2
J2BB17	10	52.3×10-6	1.011	1.031	1.045	0.437	336.2/70.1	214.9/10.7	121.7/16.6
Buqu profile 2(mean)	87	34.2×10-6	1.014	1.048	1.066	0.474	29.8/42.7	252.5/38.5	142.8/23.0
J2BC18	12	-4.432×10-6	1.061	1.122	1.201	0.154	72.5/8.3	164.2/11.7	307.8/75.6
J2BC19	11	-1.69×10-6	1.171	1.160	1.371	0.055	266.1/5.7	175.5/6.0	39.4/81.8
J2BC20	14	-1.35×10-6	-0.531	1.757	4.237	0.105	128.9/0.1	218.9/8.3	38.0/81.7
Buqu profile 3(mean)	37	-2.51×10-6	0.414	1.076	1.282	0.099	122.4/1.9	212.6/5.8	13.8/83.9

176

3 Test results

3.1 Petrographic features

3.1.1 Shamuluo Formation

Microscopic observations of the Shamuluo Formation show (Figure 2) that the main mineral composition of its sandstones consists of quartz (50-60%), feldspar (5%), mineral fragments (15-20%) and matrix (15-20%). The majority of the quartz component is derived from the clastic component and the igneous component, with the clastic quartz containing gas-liquid inclusions. The quartz of the parent rock is also irregularly residual, having been denuded during transport. The volcanic quartz is irregular, with dissolution ports and intragranular microcracks. Mineral fragments containing white mica with bright interference color in orthogonal polarization. Tuff clasts containing feldspar and quartz crystals of varying sizes. Chlorite appears pale green and pale yellow under a single polarizer. The matrix is dominated by carbonate mortar, locally showing grains of vivid interference color. In addition to quartz, the volcanic clastic rocks contain ejecta conglomerates, ejecta clasts, tuff clasts and minor inclusions of white mica and chlorite.

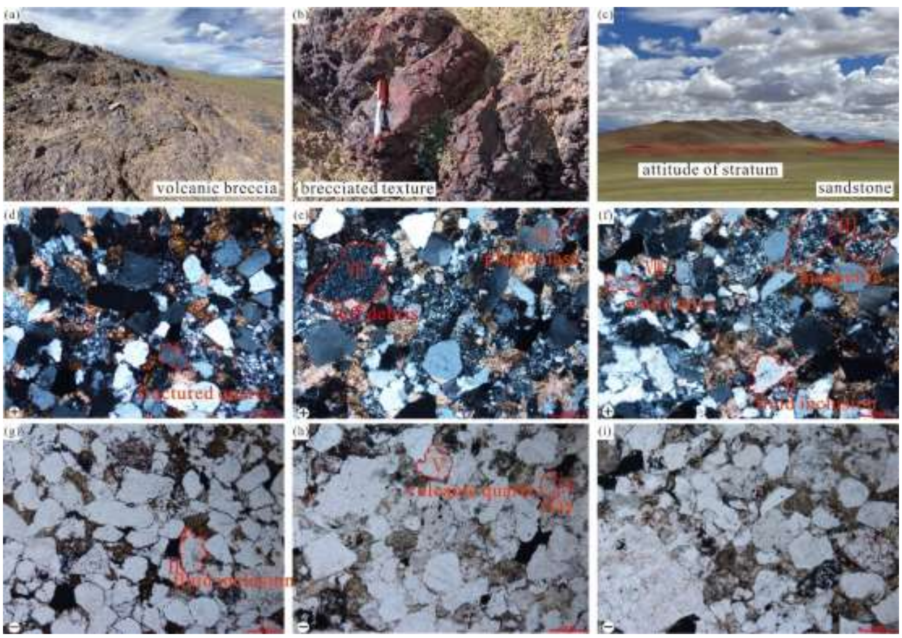

Figure 2. Field outcrops and microscopic minerals of the clastic rocks in the Shamuluo Formation. (a-c) Field outcrops of the Shamuluo Formation; (d-i) Single and orthogonal polarizing photographs of minerals.

3.1.2 Suowa Formation

Microscopic observations of the Suowa Formation show (Figure 3) that the main

https://doi.org/10.5194/egusphere-2022-1214
Preprint. Discussion started: 9 January 2023

mineral composition of the sandstone: quartz (60-70%), feldspar (5%), mineral detritus (10%) and matrix (15-25%). The quartz is mainly ‘re-rotational’ quartz and volcanic quartz. “Re-rotational” quartz has no cleavage, but has gas-liquid inclusions and regrowth. The volcanic quartz is irregularly shaped and has a dissolution edge. The feldspar type is potassium feldspar, with markedly developed cleavage. The mineral fragments are dominated by brightly colored interfering white mica, and the matrix is dominated by ejecta rock fragments, with a small amount of mudstone fragments. Ejecta rock fragments with a distinct microcrystal orientated arrangement containing dark minerals such as magnetite. The mudstone fragment is dominated by clay minerals. The mineral is severely deformed by stress and the crystals indicate visible cracks.

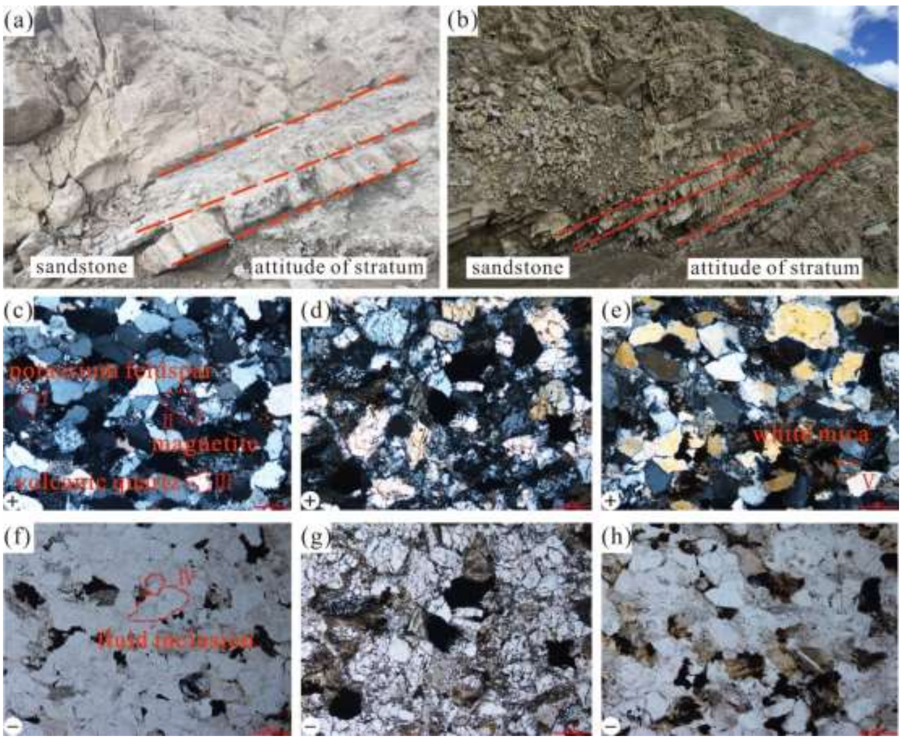

Figure 3. Field outcrops and microscopic minerals of the Suowa Formation. (a,b) Field outcrops of the Suowa Formation; (c-h) Single and orthogonal polarizing photographs of the minerals.

3.2 Zircon U-Pb chronology

3.2.1 Zircon morphological characteristics

The zircon color is mainly off-white and pale yellow, with some light red. The morphology of the zircon grains appears to be authomorphic or semi-authomorphic, with some incomplete grains exhibiting an irregular shape, possibly related to mechanical crushing during transport. The more rounded zircon grains are associated with long distance transport. The sandstone zircon grains are ellipsoidal and short-columnar, with the long axis of intact zircon grains at 100 μm and the short axis at

https://doi.org/10.5194/egusphere-2022-1214
Preprint. Discussion started: 9 January 2023

around 30-50 μm (Figure 4). Volcanic clastic zircon grains are more columnar in length, with a maximum long axis of up to 200 μm. Most zircon banding is evident, and the volcanic clastic banding pattern is more obvious than in the sandstone (Figure 5). A few shows weak bands or a greyish-bright white color with no apparent structure, associated with $Th4^{+}$ loss due to metamorphic recrystallisation. A few zircons also show a core-edge structure with oscillating rings in the core and a grey-white acyclic structure in the edge, reflecting the late growth of zircons of different genesis (Xu et al, 2010). Sandstone zircon grains have Th/U values between 0.1 and 2.1, mostly greater than 0.4 (Hermann et al, 2001). Their oscillatory rings are distinct and typical of magmatic-genetic zircons. Volcanic clastic zircon grains with Th/U values greater than 0.5 have more obvious oscillatory ring and are more influenced by magmatism.

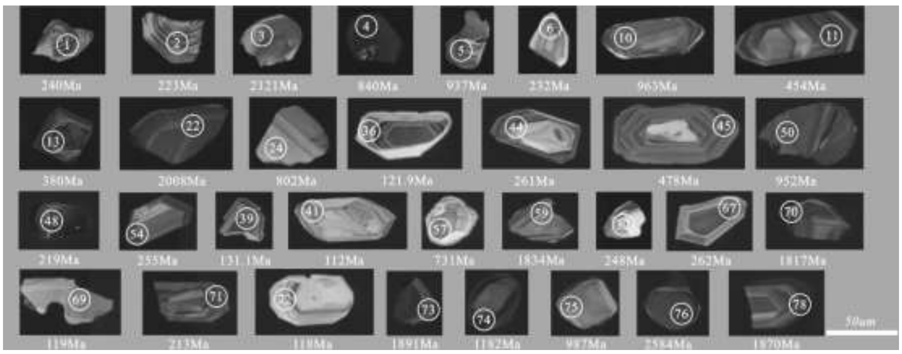

Figure 4. Representative zircon cathodoluminescence images of the sedimentary clastic rocks of the Shamuluo Formation (JS01-04).

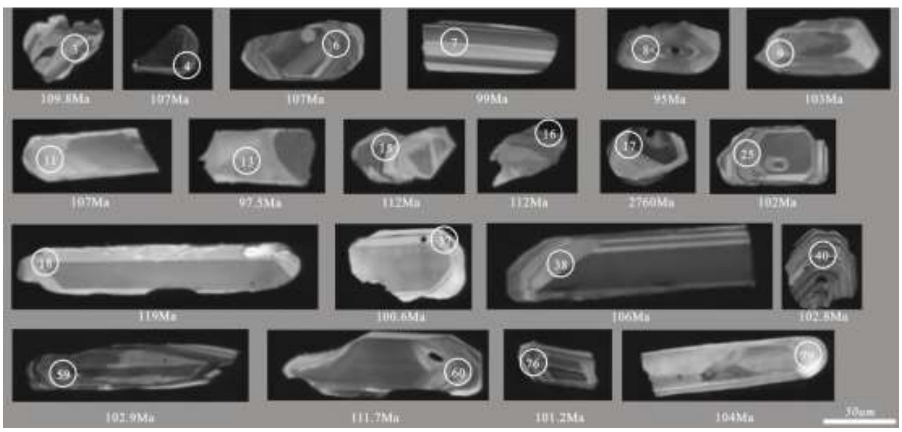

Figure 5. Representative zircon cathodoluminescence image of the volcanic breccia of the Shamuluo Formation (JS05).

3.2.2 Zircon age distribution characteristics

The youngest and oldest zircon ages obtained for the clastic sandstones are 112 Ma and 2584 Ma, respectively, and the youngest and oldest zircon ages obtained for the volcanic clastic rocks are 95 Ma and 2760 Ma, respectively. There are seven peaks in

https://doi.org/10.5194/egusphere-2022-1214
Preprint. Discussion started: 9 January 2023

clastic sandstone zircons (Figure 6(a)(b)), concentrated at 112-131 Ma, 213-380 Ma, 415-480 Ma, 627-840 Ma, 902-987 Ma, 1816-1923 Ma and 2417-2584 Ma. Volcanic clastic zircons have only one peak, concentrated at 95-116 Ma, with a weighted average age of 102.9 Ma (Figure 6(c)(d)). The histogram of the U-Pb isotopic age distribution of the zircon shows that the number of zircon grains with relatively recent ages is high in the sample. The detrital sandstone zircon grains are most abundant at 100-500 Ma, followed by 600-1000 Ma, and least abundant at 1800-2000 Ma and 2500 Ma. The volcanic clastic zircon grains are essentially all distributed at 90-120 Ma.

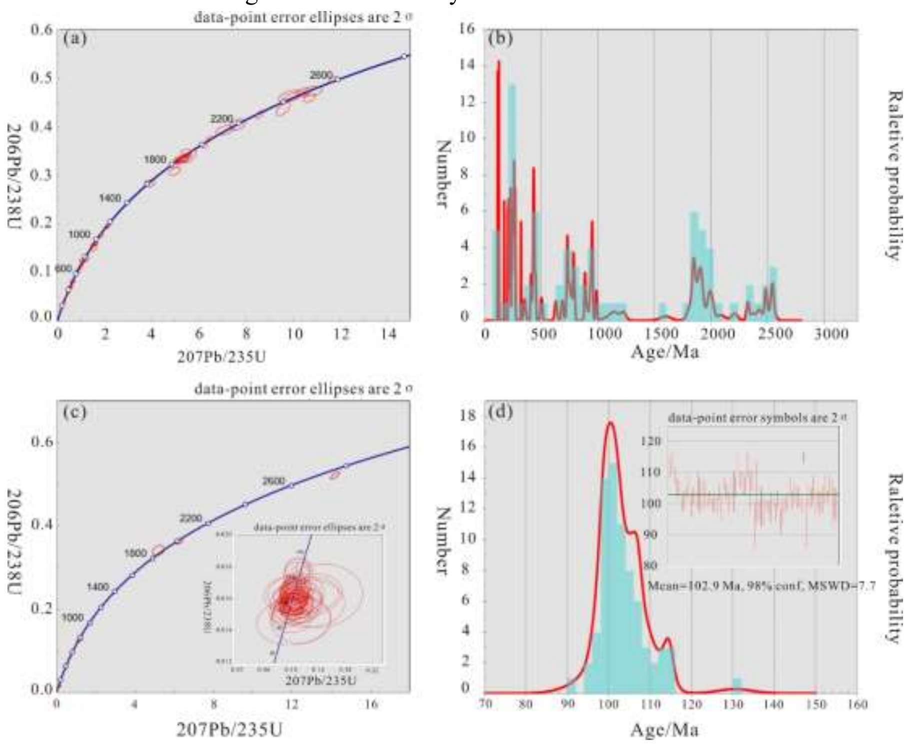

Figure 6. Zircon U-Pb dating concordant and weighted average ages of sedimentary clasts (JS01-04) and volcanic clasts (JS05) of the Shamuluo Formation. (a,b) Age concordant and distribution histograms for sedimentary clastic rocks; (c,d) Age concordance diagram and weighted mean age of volcanic clastic.

3.3 Rock magnetism

3.3.1 Variation curve of magnetization with temperature (K-T)

Different magnetic minerals exhibit different characteristics during heating and cooling, and their characteristics can be used to identify the type and size of magnetic minerals (Hrouda, 1994). K-T curves can effectively characterize the changes in magnetic minerals and their particle size during heating (Ao and Deng, 2007). The experimental results showed that the magnetization values of all samples showed a decreasing trend with increasing temperature, indicating the presence of paramagnetic

https://doi.org/10.5194/egusphere-2022-1214
Preprint. Discussion started: 9 January 2023

minerals in all samples. A significant increase in magnetization around 400°C and the appearance of peak magnetization indicates a phase change in the magnetic minerals, possibly resulting from the transformation of some of the magnetic sulfide into magnetic pyrite (Fe_3S_4). Some samples showed a significant decrease in magnetization values around 540°C, associated with the thermal decomposition of magnetic pyrite (Fe_3S_4). There were also samples where the magnetization values dropped around 580°C, indicating the presence of magnetite in the sample. The cooling curves for all samples showed a significant increase around 580°C, indicating that magnetite was produced during cooling (Figure 7). The experiments showed that the magnetic minerals in the samples were dominated by magnetite and paramagnetic minerals, while the heating and cooling process produced higher amounts of magnetite compared to the pre-experimental period.

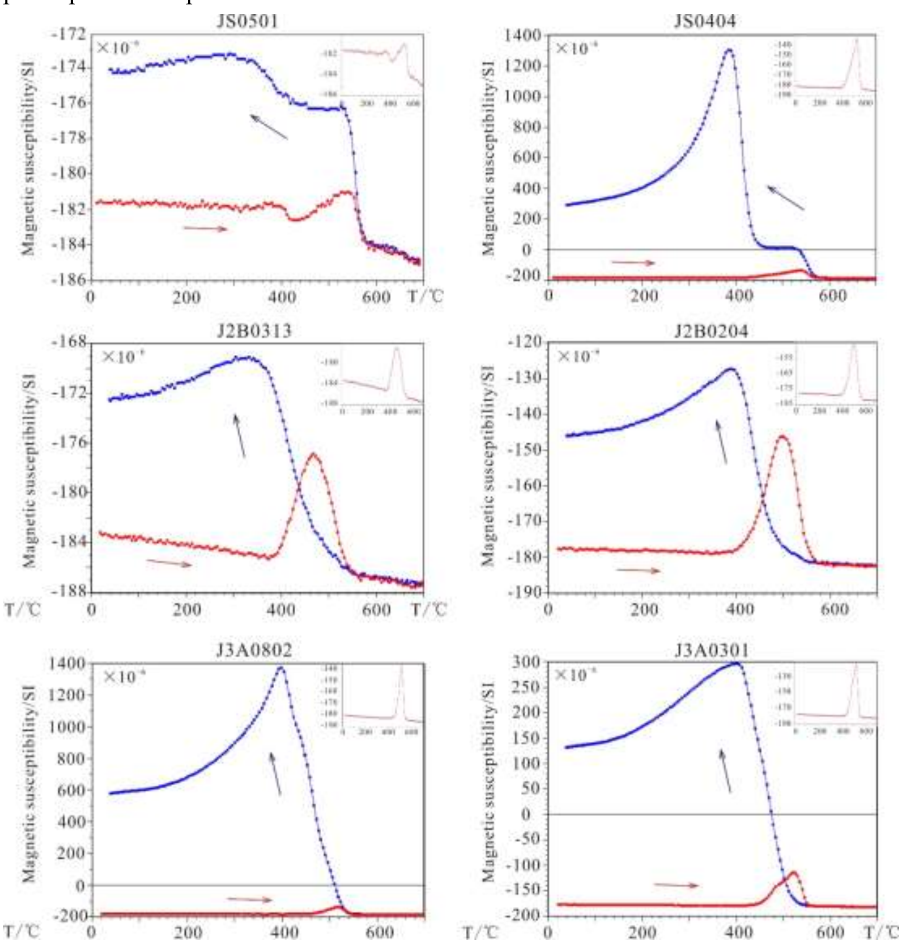

Figure 7. Variation of magnetization with temperature.

3.3.2 Saturated isothermal remanent magnetization experiment (SIRM)

The saturation isothermal remanent magnetization (SIRM) experiment uses the

https://doi.org/10.5194/egusphere-2022-1214
Preprint. Discussion started: 9 January 2023

saturation characteristic of magnetic minerals with increasing external fields to make a preliminary determination of the type of magnetic minerals in a sample. The curves for the Suowa samples show that the magnetization intensity increases rapidly with increasing external field at the beginning. When the external field strength is less than 300 mT, the magnetization intensity gradually approaches saturation, indicating that the sample is dominated by magnetic minerals with low coercivity. The magnetization intensity of the samples from the Buqu and Shamuluo Formations has not reached saturation at 2T, indicating that the magnetically loaded minerals are all relatively homogenous and dominated by high coercivity magnetic minerals. The demagnetization curves in the reverse field also indicate low coercivity for the Suowa samples and high coercivity for the Buqu and Shamuluo samples (Figure 8).

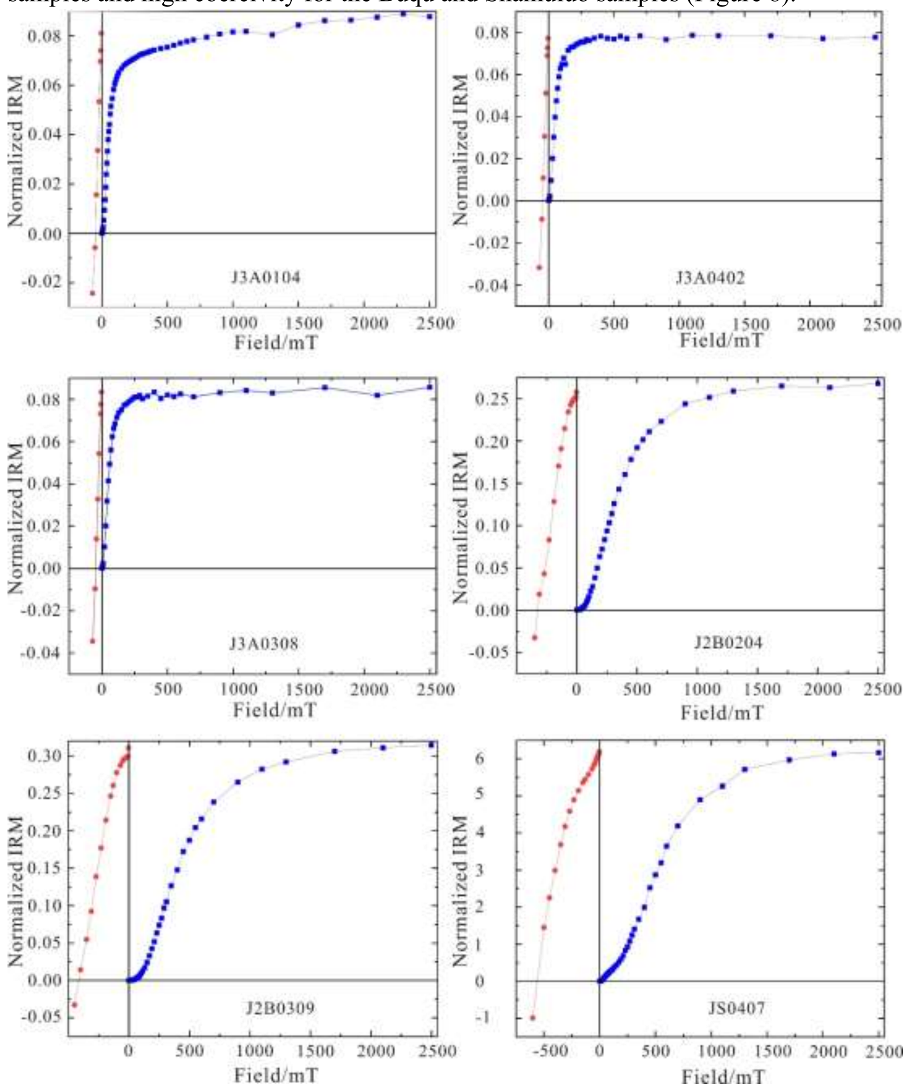

Figure 8. Curves of saturated isothermal remanent magnetization variation.

https://doi.org/10.5194/egusphere-2022-1214
Preprint. Discussion started: 9 January 2023

3.4 Magnetization and magnetic fabric characteristics

3.4.1 Magnetic fabric scalar parameters

Scalar parameters of magnetization anisotropy, including mean magnetization (Km), anisotropy (Pj), shape factor (T), maximum principal axis of magnetization (Kmax) and minimum principal axis of magnetization (Kmin), etc. Collectively, these scalars reflect magnetic fabric features (Table 1) and quantitatively characterize the degree of tectonic deformation (Tarling and Hrouda, 1993). The mean magnetization (Km) ranged from (-4.432-144) x 10^{-6}SI, exhibiting a weak magnetization rate. The Shamuluo Formation is significantly higher than the Suowa and Buqu Formations, with Km between (119-144) × 10^{-6}SI. The mean anisotropy (Pj) of the samples ranged from 0.996 to 1.282, with a relatively higher degree of strain in the Buqu Formation. Samples with strains in the Buqu and Suowa Formations have a high positive correlation between anisotropy (Pj) and the mean magnetization (Km). In contrast, the anisotropy (Pj) correlates weakly with the mean magnetization (Km) of the low-strain samples from the Suowa Formation and the undeformed samples from the Shamuluo Formation (Figure 9).

The shape factor (T) of the magnetization ellipsoid reveals the deformation mechanism of the magnetization ellipsoid, with $T > 0$ showing flattened ellipsoids and $T < 0$ showing elongated ellipsoids (Hrouda, 1982; Tarling and Hrouda, 1993). All samples from the Buqu Formation have $T > 0$ and are dominated by "flattened" ellipsoids. The samples from Profile 1 of the Suowa Formation are dominated by "elongated" ellipsoids. The sample from Profile 2 is dominated by "flattened" ellipsoids. The Shamuluo Formation samples are generally 'flattened' ellipsoids. At the same time, the Flinn diagram uses the magnetic foliation (F) and the magnetic lineation (L) parameters to distinguish the shape of the magnetization ellipsoid in terms of ellipticity (E). The results are consistent with the ellipsoidal morphology of the magnetization reflected by the shape factor (T) (Figure 9).

Pj-T diagrams provide a diagenetic analysis of the degree of deformation of rocks during tectonics (Jelinek, 1981; Hrouda, 1982). The magnetization ellipsoid moves from oblate to oblong to oblate, undergoing a process from sedimentary to tectonic (Borradaile and Henry, 1997). The transition of the ellipsoid from oblate to oblong, indicating the evolution of deformed sediments to palaeocurrent-disturbed or weakly deformed sediments. The evolution of oblong to oblate indicates the evolution of moderately deformed sediments to strongly deformed sediments (Wang et al, 2017). Samples from profiles 1 and 2 of the Buqu Formation, which exhibit a flattened ellipsoid, may be primary deposits or strongly deformed sediments. Samples from profile 3 of the Buqu Formation, with ellipsoids that are both oblate and oblong, may contain deformation processes ranging from primitive deposition to strong deformation, and possibly moderate to strong deformation. The samples from profile 1 of the Suowa Formation have predominantly oblate ellipsoids, suggesting moderate or strong tectonic deformation. The samples from profile 2 of the Suowa Formation has 60% of the ellipsoid as oblate and the other as oblong. It may be primitive deposition to

https://doi.org/10.5194/egusphere-2022-1214
Preprint. Discussion started: 9 January 2023

palaeocurrent or weak deformation processes, or moderate to strong deformation processes. The ellipsoid of the Shamuluo Formation samples is oblate and may be primitive deposition or a strong deformation process (Figure 9).

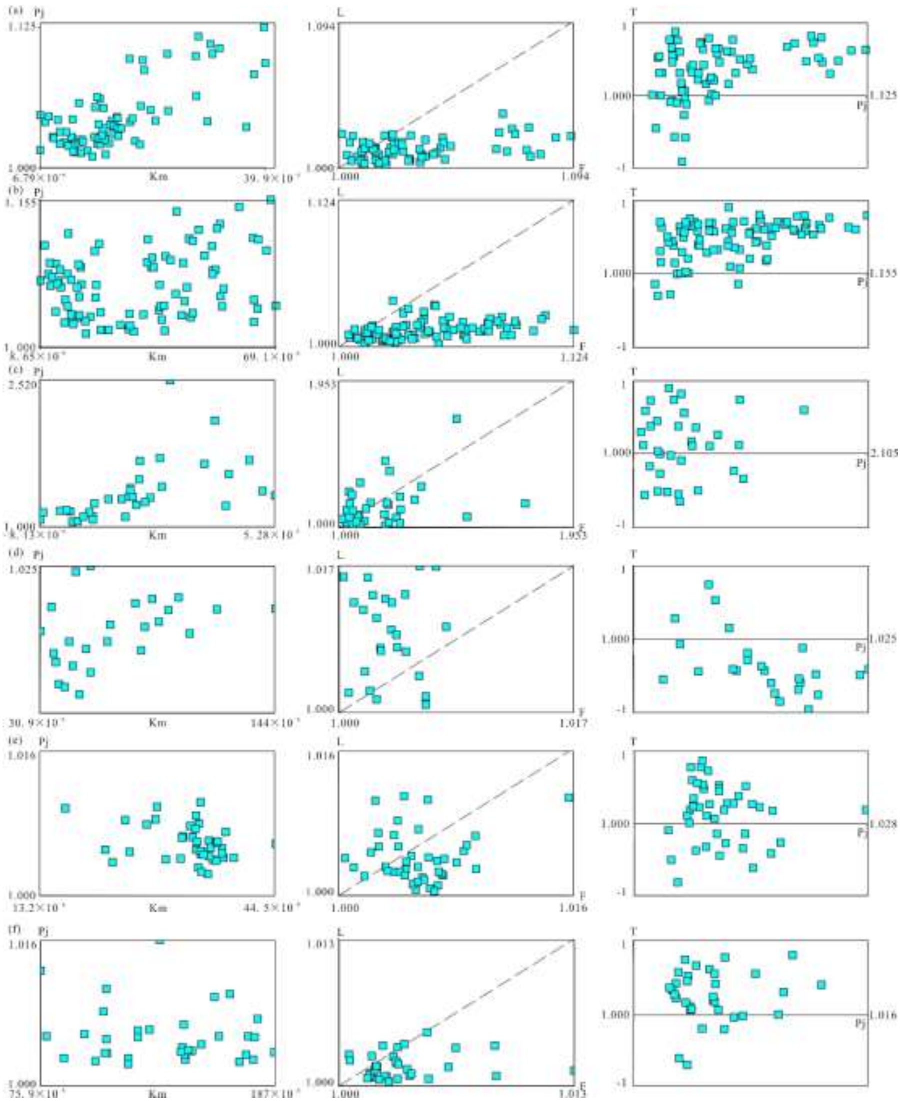

Figure 9. Diagram of magnetic fabric scalar parameter. (a) Profile 1 of Buqu Formation; (b) Profile 2 of Buqu Formation; (c) Profile 3 of Buqu Formation; (d) Profile 1 of Suowa Formation; (e) Profile 2 of Suowa Formation; (f) Profile of Shamuluo Formation.

3.4.2 Orientation of the main axis of the magnetization ellipsoid

Magnetization ellipsoids in deformed rocks correspond well to strain ellipsoids (Wu, 1988; Tarling and Hrouda, 1993) and can reflect the dominant occurrence of the rock.

1. Buqu Formation Profile

The equatorial projection of the main axis of magnetization of the Profile 1 shows that the magnetic lineation represented by the axis of maximum magnetization (Kmax) is distributed in quadrants one, two and three and near the X axis, with a SW-NE direction of dominance and a dominant occurrence of 27.7°∠18.2° with a relatively small inclination angle. The minimum magnetization principal axis (Kmin) is projected equatorially mainly in the second and fourth quadrants and near the Y-axis, with the dominant direction being near NW-SE, the dominant occurrence being 143.2°∠52.7° and the inclination angle being relatively large, reflecting the extrusion stress in the NW-SE direction. The equatorial projection of the main axis of magnetization of the Profile 2 shows that the magnetic lineation represented by the axis of maximum magnetization (Kmax) is distributed in quadrants three and four and near the X-axis, with a dominant direction of WE and a dominant occurrence of 29.8° ∠ 42.7°, with a relatively small inclination angle. The minimum magnetization principal axis (Kmin) is projected equatorially in the second and fourth quadrants and near the Y-axis, with the dominant direction being NW-SE, the dominant occurrence of 142.8°∠23° and a relatively large inclination angle, reflecting the extrusion stresses of NW-SE. The equatorial projection of the main axis of magnetization for the Profile 3 shows a scattered distribution of the axis of maximum magnetization (Kmax) with a dominant occurrence of 122.4°∠1.9° and a relatively large inclination angle. The minimum magnetization principal axis (Kmin) is concentrated near the center of the circle, reflecting the magnetic fabric of the low deformation (Figure 10).

2. Suowa Formation Profile

The equatorial projection of the main axis of magnetization of the Profile 1 shows that the axis of maximum magnetization (Kmax) is projected near the center of the circle in the dominant NE-SW direction, with a dominant occurrence of 88.9° ∠ 77.3° and a large inclination angle. The minimum magnetization principal axis (Kmin) is distributed in quadrants one, three and four, but reflect a dominant direction of 184.6° ∠ 1.3°, indicating extrusion stresses subject to NE-SW. The equatorial projection of the maximum axis of magnetization (Kmax) for the Profile 2 is in quadrants two and three, and shows a scattered distribution unlike the high strain samples. The minimum magnetization principal axis is concentrated near the center of the circle in the fourth quadrant, exhibiting a low degree of deformation in the magnetic fabric (Figure 10).

3. Shamuluo Formation Profile

The equatorial projection of the main axis of magnetization of the Shamuluo Formation samples shows that the axis of maximum magnetization (Kmax) is scattered in all quadrants and the axis of minimum magnetization (Kmin) is concentrated near the center of the circle, reflecting a low-deformation magnetic fabric. Compared to the low-deformation samples of the Suowa Formation, the minimum magnetization axis of the Shamuluo Formation is more concentrated in the center of the circle, and the maximum magnetization axis is more scattered and less strained (Figure 10)

https://doi.org/10.5194/egusphere-2022-1214
Preprint. Discussion started: 9 January 2023

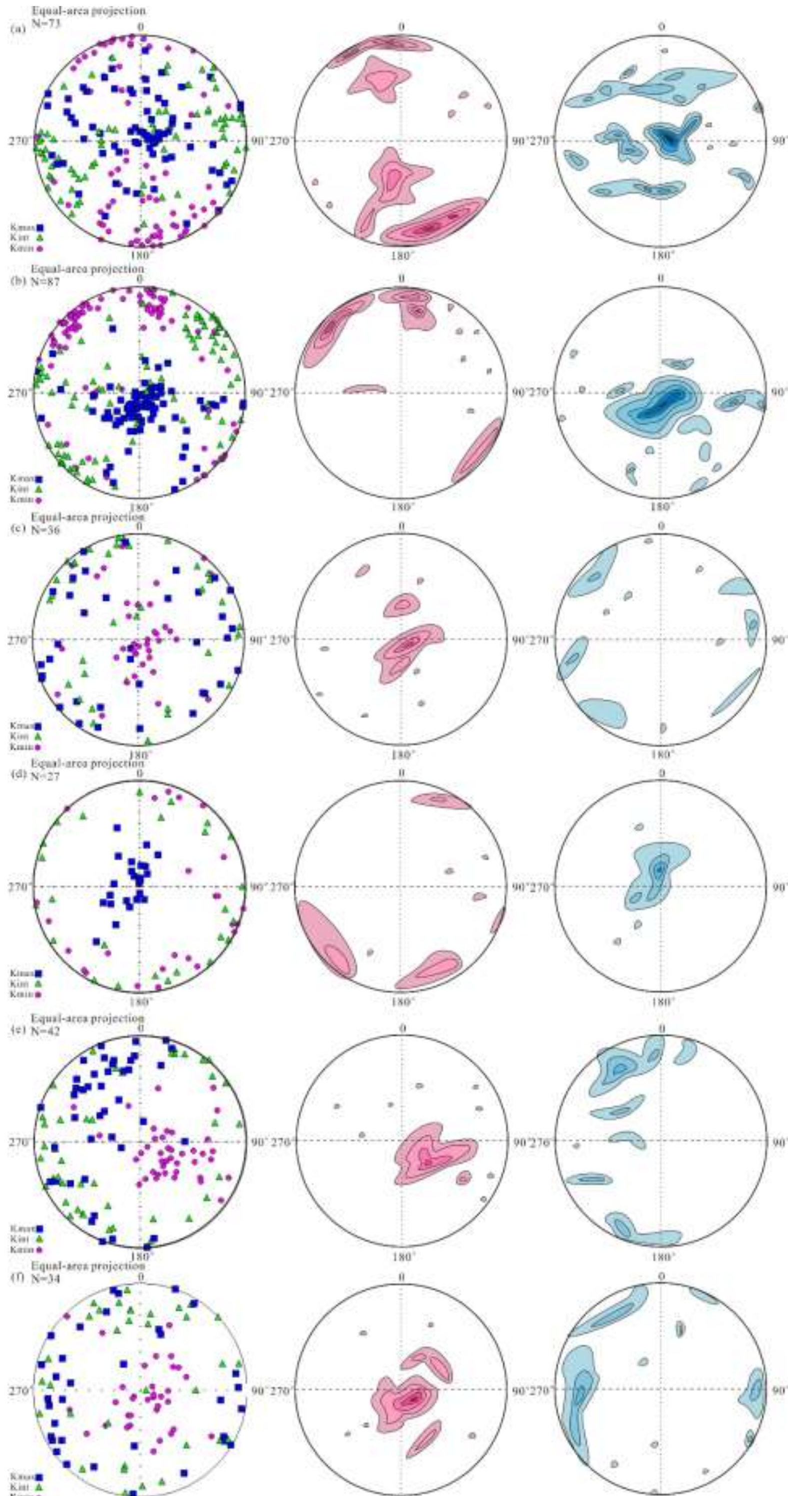

https://doi.org/10.5194/egusphere-2022-1214
Preprint. Discussion started: 9 January 2023

Fig. 10. Equatorial projection of the main axis of magnetization. (a) Profile 1 of Buqu Formation; (b) Profile 2 of Buqu Formation; (c) Profile 3 of Buqu Formation; (d) Profile 1 of Suowa Formation; (e) Profile 2 of Suowa Formation; (f) Profile of Shamuluo Formation.

4 Discussion

4.1 Stratigraphic time sequence of the Shamuluo Formation with the Buqu and Sowa Formations

The Shamuluo Formation belonging to Late Jurassic-Early Cretaceous is exposed in the Ban-Nu Suture Zone and is representative of residual marine deposits. The Buqu and Suowa Formations belonging to Middle-Late Jurassic are exposed in the South Qiangtang Massif and represent the marine deposits of the Qiangtang Massif during the Jurassic. The division of the temporal sequence of the three strata is essential to constrain the sequence of tectonic events. The Shamuluo Formation is considered to belong to the Late Jurassic-Early Cretaceous by the biological fossils found in the Ban -Nu Suture Zone ((Xie et al, 2009; Xie et al, 2010; Deng, et al, 2017). Previously obtained detrital zircon ages similarly indicate its formation in the Late Jurassic-Early Cretaceous (Huang et al, 2017; Wu et al, 2021). According to the detrital zircon dating study in this paper, the Shamuluo Formation in the central part of the suture zone is Early Cretaceous.

The temporal limit of the Buqu Formation is not much disputed and is generally considered to be Bathonian Stage, Middle Jurassic. Fossil and climatic studies of the lower part of the Suowa Formation suggest that it belongs to the Oxford Stage (163.5 Ma-157.3 Ma), Late Jurassic (Zeng et al, 2021). Ammonites from the upper part suggest a Tithonian Stage, Late Jurassic (Song et al, 2016). It has also been suggested that the upper part of the Suowa Formation belongs to the Late Jurassic-Early Cretaceous (Fu et al, 2021; Zeng et al, 2021). For example, the 151±2 Ma granodiorite dikes intruding the Shamuluo Formation (Ma et al, 2018) and the 143 Ma and 163 Ma Shamuluo Formation clastic rocks (Li et al, 2017) suggest a possible diachronism match with the Shamuluo Formation. However, based on the age of the Shamuluo Formation in this paper, it can be assumed that the Suowa Formation was deposited earlier than the Shamuluo Formation (Figure 11).

https://doi.org/10.5194/egusphere-2022-1214
Preprint. Discussion started: 9 January 2023

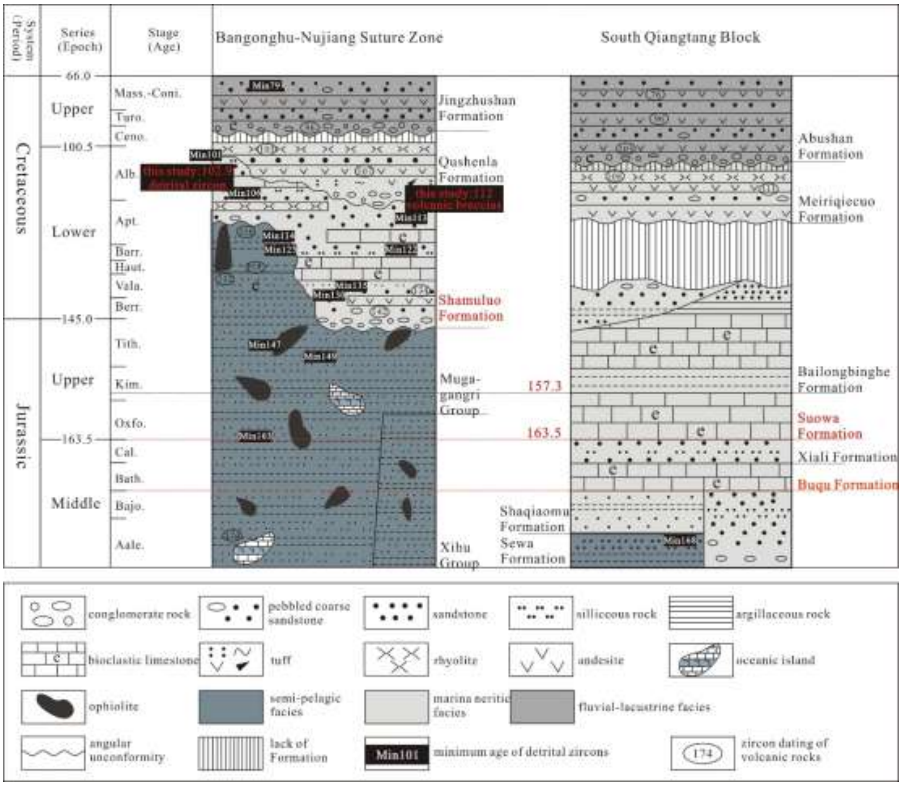

Fig. 11. Comparison of the stratigraphic sequence of the Shamuluo Formation with the Buqu and Suowa Formations.

4.2 Influence of magnetically loaded minerals on magnetic fabric parameters

The sandstones of the Shamuluo Formation have Km values of (119-144) x 10^{-6}SI, which are higher than those of the Suowa Formation. Rock magnetism experiments indicate that the magnetically loaded minerals in both are dominated by magnetite and paramagnetic minerals. Mineral microscopy shows more magnetite in the Shamuluo Formation than in the Suowa Formation. Paramagnetic minerals, mainly including white mica and chlorite, are also more abundant in the Shamuluo Formation. In addition, diamagnetic minerals like quartz and feldspar are somewhat more abundant in the Suowa Formation. Km values for the Buqu Formation are relatively low, but negative values are also present. Among the carbonate minerals, the main contributors to the Km values should be the paramagnetic mineral and the diamagnetic mineral, such as calcite. It is certain that the limestone sample with a negative Km has calcite as the absolute contributor and that this sample has a higher Fe content in the calcite, resulting in a relatively large Pj (Schmidt et al, 2006). For most deformed rocks, Pj values generally range from 1.05 to 2.5 (Pares, 2004). The sandstone samples of the Shamuluo Formation, with a mean Pj of 1.005, are undeformed rocks. All samples are Fe-bearing silicate minerals, with the exception of a limestone sample from profile 3 of the Buqu Formation, where Pj is greater than 1.35 (Jelinek, 1981). Pj is greater than 1.35 in the third profile of the Buqu Formation, suggesting a decisive influence of ferromagnetic minerals (Hrouda, 2010). For T values, silicate minerals are the main contributors to the AMS when $0 \leq T \leq 1$ (Cao, 2022). All samples have T values > 0 except for profile 1 of the Suowa Formation, which has T values < 0, thus confirming the contribution of silicate minerals.

4.3 Magnetic fabric types and tectonic movements revealed

Previous explorations of the evolution of sedimentary rock magnetic fabrics have suggested the existence of five strain fabrics following tectonic deformation of sedimentary rocks (Pares et al, 1999; Saint-Bezar et al, 2002; Luo et al, 2009). Based on the orientation of the main axis of the magnetic fabric, combined with the Flinn and Pj-T diagrams, it is suggested that the samples from the Buqu Formation (profiles 1 and 2) are all strongly cleaved magnetic fabric and that profile 3 is a transition from the original sedimentary fabric to the initial deformation fabric. The samples from the Suowa Formation (Profile 1) are of tensile lineation magnetic fabric, the samples from the Suowa Formation (Profile 2) are of initial deformation magnetic fabric, and the samples from the Shamuluo Formation are of primitive sedimentary magnetic fabric. The initial deformation magnetic fabric of the Suowa Formation (Profile 2) has a more concentrated Kmax distribution and spreads along the strike of the formation, suggesting that it formed in an extrusive environment (Borradaile and Hamilton, 2004; Cifelli et al, 2005). The tensile lineation magnetic fabric of the Suowa Formation (Profile 1), with Kmax perpendicular to the level and the direction of the magnetic fabric parallel to the direction of minimum principal stress, suggests that it formed in a tensile environment (Faccenna et al, 2002). In addition, the strongly cleaved magnetic fabric in profiles 1 and 2 of the Buqu Formation, which have the same magnetic lineation direction parallel to the direction of minimum principal stress, are formed in a tensile environment (Figure 10).

The magnetic fabric was closed early in the orogeny, and during general tectonic deformation, the magnetic fabric acquired early in the orogeny was rotated with the strata during later deformation (Larrasonana et al, 2004; Garaica-Lasanta et al, 2015), so the magnetic lineation should record the direction of the rotated palaeostress field (Scheepers and Langereis, 1994). The strongly cleaved magnetic fabric of the Buqu Formation, with its magnetic lineation directions of SW-NE and WE, respectively, may correspond to the direction of the paleostress field during rotation. In contrast, the tensile lineation magnetic fabric of the Suowa Formation, which has a SW-NE direction, also corresponds to the direction of the palaeostress field (Figure 10). This suggests that the Qiangtang Terrane may have undergone an anticlockwise rotation from WE to SW-NE orientation during the diagenetic phase from the Buqu Formation to the Suowa Formation.

4.4 Relationships between magnetic fabric and fracture movement

https://doi.org/10.5194/egusphere-2022-1214
Preprint. Discussion started: 9 January 2023

Since the magnetization ellipsoid of strained rocks corresponds well to the strain ellipsoid (Borradadile, 1988; Wu, 1988), the axis of minimum magnetization ellipsoid (Kmin) represents the axis of compression of maximum strain, which is the direction of maximum extrusion stress (Tarling and Hrouda, 1993). Therefore, this dominant direction is defined as the extrusion stress vector R, which is decomposed into stress components N and P along its horizontal and vertical directions, and the relationship between the two is analyzed kinematically (Lu et al, 2008; Wang et al, 2017).

The two strongly cleaved magnetic fabric profiles of the Buqu Formation, where the fractures are located, are both WE trending and both have a minimum magnetization axis azimuth of about 140°. Therefore, a result is used instead of the vector decomposition of its main axis azimuth. Vector decomposition of the azimuth of the minimum magnetization principal axis in the horizontal plane along the fracture strike and vertical fracture strike (Figure 12). The results indicate that there is a sinistral movement of anticlockwise rotation in the horizontal plane along the strike of the fracture with a large component, indicating the presence of a relatively strong sinistral movement in the Buqu Formation. The same vectorial decomposition is performed for the tensile lineation magnetic fabric and the initial deformed magnetic fabric of the Suowa Formation (Figure 12). The results show that the same anticlockwise sinistral movement is present in the tensile lineation magnetic fabric, but its fraction is relatively reduced and the intensity of the possible sinistral slip is reduced. However, the initial deformed magnetic fabric samples exhibit a clockwise dextral movement with a relatively large component, indicating the presence of a relatively strong dextral movement.

For relatively continuous strata, there is a characteristic of levorotation and then dextrorotation, and the components change from strong to weak and then to strong. Combined with the anticlockwise rotation from WE to SW-NE that existed during the period from the Buqu Formation to the Suowa Formation as reflected by the palaeostress field. As well as the initial deformation magnetic fabric of the Suowa Formation, which occurred in the extrusion environment, and its tensile lineation magnetic fabric and the strongly cleaved magnetic fabric of the Buqu Formation occurred in the tension environment. Together, these three evidences suggest an extrusive tectonic setting from the Buqu Formation to the Suowa Formation as a result of the anticlockwise movement occurring in the South Qiangtang Massif. With this the anticlockwise movement stopped and the terrane began to rotate clockwise, producing a tensile tectonic environment accordingly. The upper part of the Suowa Formation may be the boundary between the two tectonic settings, and its origin is closely related to the subduction and closure of the BangongCo-Nujiang Tethys Ocean. It is possible that the subduction polarity of the Ban-Nu Tethys Ocean has changed, causing a change in the direction of plate rotation.

https://doi.org/10.5194/egusphere-2022-1214
Preprint. Discussion started: 9 January 2023

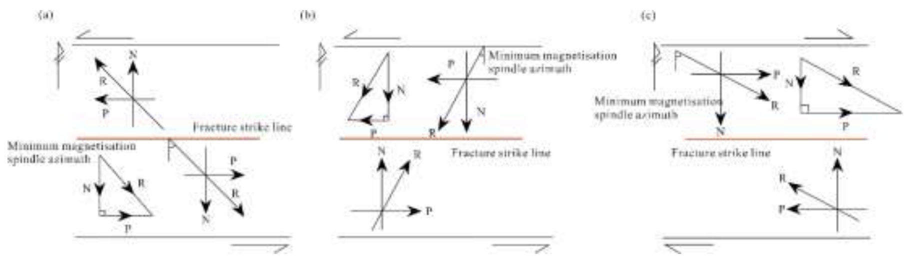

Figure 12. Analysis of magnetic fabric on fracture movement. (a) Profiles 1 and 2 of Buqu Formation, strongly cleaved magnetic fabric; (b) Profile 1 of Suowa Formation, tensile lineation magnetic fabric; (c) Profile 2 of Suowa Formation, initial deformed magnetic fabric.

4.5 Timing of closure and subduction polarity transition in the BangongCo-Nujiang Tethys Ocean

Studies on the time frame and mode of closure of the BangongCo-Nujiang Tethys Ocean have mainly focused on the views of "diachronism closure" and "scissor collision", with closure times from east to west of 116.6 ± 0.8 Ma, 120 ± 1.4 Ma, 107.8 ± 8.1 Ma, and 96.0 ± 1.1 Ma, respectively (Fan et al, 2015; Wu et al, 2016). We believe that at least in the middle of the suture zone, the Ban-Nu Ocean is closing and is in the late stages of closure. The view comes from the following points, the source area analysis suggests that the central and northern parts of the Lhasa Terrane, as well as the South Qiangtang Massif, are potential sources for the Shamuluo Formation. The exchange of material between the Lhasa Terrane, the Qiangtang Massif and the Suture Zone marks the disappearance of the deep-sea shelf. Magnetic fabric studies indicate that the sandstones of the Shamuluo Formation belong to a primitive sedimentary magnetic fabric, marking a relatively stable depositional environment. Compared with the deformed magnetic fabrics of the Buqu and Suowa Formations, this suggests that strong tectonic events have been reduced. However, the 102.9 Ma age of the volcanic rocks of the Shamuluo Formation again suggests that a tectonic thermal event still existed at this time. In addition, a paleomagnetic comparison of the South Qiangtang Massif (Cheng et al, 2012; Chen et al, 2017; Cao et al, 2018) and the Lhasa Terrane (Zhou et al, 2016; Li et al, 2016, 2017; Ma et al, 2017; Cao et al, 2017; Bian et al, 2017) for their Mesozoic paleolatitudinal positions (Figure 13), suggesting that the two terranes began to collapse at 150 Ma and achieved collapse at 145 Ma, thus implying the closure of the BangongCo-Nujiang Tethys Ocean. The synthesis suggests that the closure of the BangongCo-Nujiang Tethys Ocean should be limited to after 109.9-131 Ma, when the degree of closure is nearing its end.

https://doi.org/10.5194/egusphere-2022-1214
Preprint. Discussion started: 9 January 2023

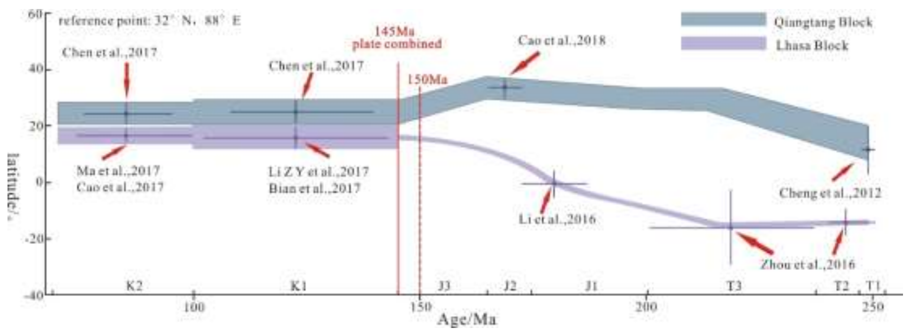

Figure 13. Paleolatitude changes and closure times since the Triassic in the Lhasa and Qiangtang Terranes (Sun et al, 2019).

Changes in the polarity of oceanic subduction are caused by the upwelling of the asthenosphere due to plate reversal to breakage (Gvirtzman and Nur, 1999; Tatsumi, 2006; Grove et al, 2009). There are various views on the subduction polarity of the BangongCo-Nujiang Tethys Ocean. In the mainstream view of bidirectional subduction, evidence includes the Biluocuo fore-arc basin in the South Qiangtang Massif (Ma et al, 2017), the Lalang ophiolite, and the formation of the Ban-Nu Suture Zone and the Shiquan River-NamuCo-Bomi Suture Zone (Zhu et al, 2009, 2011, 2013; Sui et al, 2013).

Current research suggests that the Ban-Nu Ocean was subducted southward prior to the late Suowa Formation of the South Qiangtang Massif (163.5-157.3 Ma). Evidence to support this conclusion is that the period corresponds to the Oxfordian Age when global sea level fell but the Qiangtang Basin was a regional sea level rise. The cause of this event would be the southward subduction of the Ban-Nu Ocean, resulting in a regional subsidence rate greater than the global rate of sea level fall, corresponding to the extensional tectonic setting of the Qiangtang Massif. The extensional tectonic setting of the strongly magnetic fabric of the Buqu Formation and the tensile lineation magnetic fabric of the Suowa Formation may be responsible for the anticlockwise rotation of the South Qiangtang Massif. The clockwise rotation of the terrane, as revealed by the initial deformed magnetic fabric of the Suowa Formation, and the creation of an extrusive tectonic setting, suggest that a change in subduction polarity occurred in the Ban-Nu Ocean during the late Suowa Formation, when northward subduction began. In addition, the detrital zircons of the Shamuluo Formation in this paper reveal that the main body of the sample is in a collisional tectonic setting and a few in a convergent tectonic setting, with the convergent setting occurring prior to the collisional setting (Figure 14). This method reflects the different tectonic settings of the sedimentary basins in which the detrital zircons are located by the difference between the crystalline age of the detrital zircons and the age of the sedimentary strata (Cawood et al, 2012). The convergent and collisional settings reflect an orogenic collisional event between the Ban-Nu Suture Zone and the South Qiangtang Massif. This also suggests that the Early Cretaceous, in which the Shamuluo Formation is located in this paper, would have been the later stage of the merging of the BangongCo-Nujiang Tethys

https://doi.org/10.5194/egusphere-2022-1214
Preprint. Discussion started: 9 January 2023

Ocean with the South Qiangtang Massif.

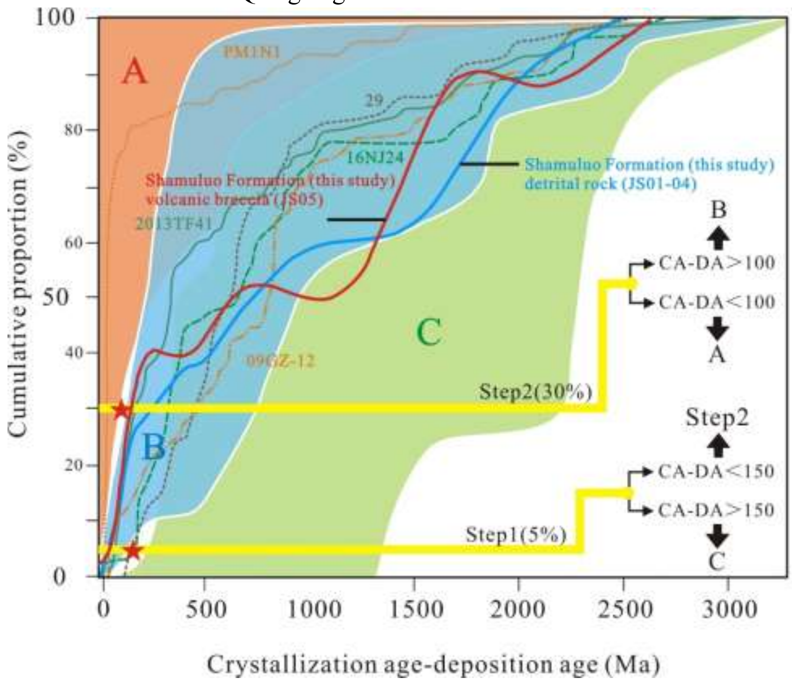

Figure 14. Differences in zircon crystallization age and sedimentation age between different tectonic settings in the Shamuluo Formation.

5 Conclusion

The following conclusions can be given, after carrying out the previous study of rock magnetism, magnetic fabric and zircon U-Pb chronology.

(1) Zircon U-Pb chronology of the Shamuluo formation exposed in the Ban-Nu Suture Zone indicates a weighted mean age of 102.9 Ma for the volcanic clastic rocks and a youngest age of 112-31 Ma for the sedimentary clastic rocks, belonging to the Late Jurassic-Early Cretaceous.

(2) In all samples. the magnetically loaded minerals were made up of magnetite, paramagnetic and diamagnetic minerals. The majority ingredient of the Shamuluo Formation is magnetite and paramagnetic minerals, and the remains is quartz and feldspar. The Suowa Formation is consistent with the Shamuluo Formation, but with less magnetite and more quartz and feldspar. The limestone of Buqu Formation is dominated by silicate minerals, some of which are with high iron content, leading to the high value of Pj.

(3) Among the strain magnetic fabrics of all samples, the strongly cleaved magnetic fabric of the Buqu Formation, the tensile lineation magnetic fabric of the Suowa Formation and the initial deformed magnetic fabric reveal anticlockwise sinistral and clockwise dextral movements, respectively. Thus, it indicates that the direction

of rotation of the South Qiangtang Massif changed from the Middle Jurassic to the Late Jurassic, possibly related to a change in the subduction polarity of the BangongCo-Nujiang Tethys Ocean. In addition, the Late Jurassic-Early Cretaceous Shamuluo Formation, which developed a primitive sedimentary magnetic fabric, may mark the imminent end of closure of the Ban-Nu Tethys Ocean.

(4) The BangongCo-Nujiang Tethys Ocean has been subducting southwards until the late Suowa Formation (163.5-157.3 Ma) and then changes its direction to northwards. Afterwards, it started to close at 145 Ma and stopped subduction at 131-109.9Ma.

Competing interests

The authors declare that they have no conflict of interest.

Team list

Hanning Wu (State Key Laboratory of Continental Dynamics, Department of Geology, Northwest University, 710069, China), Xin Cheng (State Key Laboratory of Continental Dynamics, Department of Geology, Northwest University, 710069, China), Feifei Huo (College of Engineering, Zunyi Normal University, Zunyi Guizhou 563006, China), Yannan Zhou (State Key Laboratory of Continental Dynamics, Department of Geology, Northwest University, 710069, China), Nan Jiang (College of Petrol and Environment Engineering, Yan'an University, Yan'an 716000, Shaanxi, China), Qinglong Chen ((State Key Laboratory of Continental Dynamics, Department of Geology, Northwest University, 710069, China), Bitian Wei (State Key Laboratory of Continental Dynamics, Department of Geology, Northwest University, 710069, China), Dongmeng Zhang (State Key Laboratory of Continental Dynamics, Department of Geology, Northwest University, 710069, China), Longyun Xing (State Key Laboratory of Continental Dynamics, Department of Geology, Northwest University, 710069, China), Teng Li (State Key Laboratory of Continental Dynamics, Department of Geology, Northwest University, 710069, China), Feifan Liu (State Key Laboratory of Continental Dynamics, Department of Geology, Northwest University, 710069, China), Xiaohong Deng (State Key Laboratory of Continental Dynamics, Department of Geology, Northwest University, 710069, China), Shuqi Lan (State Key Laboratory of Continental Dynamics, Department of Geology, Northwest University, 710069, China), Jingyue Wu (State Key Laboratory of Continental Dynamics, Department of Geology, Northwest University, 710069, China), Jiawei Wang (State Key Laboratory of Continental Dynamics, Department of Geology, Northwest University, 710069, China), Baofeng Wang (Gansu Provincial Coal Geological Exploration Institute, Lanzhou 730000, China), Pengxiang Xu (Gansu Provincial Coal Geological Exploration Institute, Lanzhou 730000, China).

https://doi.org/10.5194/egusphere-2022-1214
Preprint. Discussion started: 9 January 2023

Author Contributions

Qinglong Chen proposed the study; sampled in the field; analyzed the data; designed the figures; collected the data and evidence; and wrote the initial draft. Hanning Wu provided funding support; supervised the execution; and managed the research planning. Xin Cheng managed the data. Feifei Huo analyzed the study data. Yanan Zhou conducted the research process. Nan Jiang designed the methodology. Bitian Wei sampled in the field; and tested the software. Baofeng Wang sampled in the field. Pengxiang Xu sampled in the field. Dongmeng Zhang sampled in the field; tested the software. Longyun Xing sampled in the field. Teng Li sampled in the field. Feifan Liu sampled in the field. Jingyue Wu sampled in the field. Jiawei Wang sampled in the field.

https://doi.org/10.5194/egusphere-2022-1214
Preprint. Discussion started: 9 January 2023

References

Ao, H., and Deng, C.L.: Review in the identification of magnetic minerals, PROGRESS IN GEOPHYSICS.,22, 432-442, https://doi.10.3969/j.ssn.1004-2903.2007.02.015, 2007.

Bian, W., Yang, T., Ma, Y., et al.: New early Cretaceous paleomagnetic and geochronological results from the far western Lhasa terrane: Contributions to the Lhasa-Qiangtang collision, Sci. rep-uk., 7, 16216, https://doi.org/10.1038/s41598-017-16482-3, 2017.

Borradaile, G. J.: Magnetic susceptibility, petrofabrics and strain, Tectonophysics., 156, 1-20, https://doi.org/10.1016/0040-1951(88)90279-X, 1988.

Borradaile, G. J., and Henry, B.: Tectonic applications of magnetic susceptibility and its anisotropy, Earth-sci. rev., 42, 49-93, https://doi.10.1016/S0012-8252(96)00044-X, 1997.

Borradaile, G. J., and Hamilton, T.: Magnetic fabrics may proxy as neotectonic stress trajectories, Polis rift, Cyprus, Tectonics., 23, TC1001, https://doi.org/10.1029/2002TC001434, 2004.

Cao, X. W., Sun, Z. M., Huang, B. C., et al.: Magnetic fabric separation and analysis of rock tectonic deformation, Chinese J. Geophys., 65, 448-470, https://doi.10.6038/cjg2022P0336, 2022.

Cao, Y., Sun, Z. M., Li, H. B., et al.: New Late Cretaceous paleomagnetic data from volcanic rocks and red beds from the Lhasa terrane and its implications for the paleolatitude of the southern margin of Asia prior to the collision with India, Gondwana res., 41, 337-351, https://doi.org/10.1016/j.gr.2005.11.006, 2017.

Cao, Y., Sun, Z. M., Li, H. B., et al.: New paleomagnetic results from Middle Jurassic limestones of the Qiangtang terrane, Tibet: Constraints on the evolution of the Bangong-Nujiang Ocean, Teconics., 38, 215-232, https://doi.org/10.1029/2017TC004842, 2018.

Chen, W., Zhang, S., Ding, J., et al.: Combined paleomagnetic and geochronology study on Cretaceous strata of the Qiangtang terrane, central Tibet, Gondwana res., 41, 93-109, https://doi.org/10.1016/j.gr.2015.07.004, 2017.

Cheng, X., Wu, H. N., Diao, B. G., and et al.: New paleomagnetic result of the Middle-Late Jurassic rocks from the northern Qiangtang Block, west China, Chinese J. Geophys., 55, 3399-3409, https://doi.10.6038/j.ossn.0001-5733.2012.10.023, 2012.

Cifelli, F., Mattei, M., Chadima, M., Hirt, A. M., and Hansen, A.: The origin of tectonic lineation extensional basins: Combined neutron texture and magnetic analyses on "undeformed" clays, Earth planet sc lett., 235, 62-78, https://doi.org/10.1016/j.epsl.2005.02.042, 2005.

Deng, J. H., Yuan, Z. G., Yu, Jiang., Du, C. F., et al.: New discovery of the Basal Conglomerate in the Upper Jurassic-Lower Cretaceous Shamuluo Formation in Western part of Bangong Lake-Nujiang River Suture Zone and its geological significance, Geol. Rev., 63, 302-310, 2017.

Fan, J. J., Li, C., Xie, C. M., et al.: The Evolution of the Bangong-Nujiang Neo-Tethys

https://doi.org/10.5194/egusphere-2022-1214
Preprint. Discussion started: 9 January 2023

Ocean: Evidence from Zircon U-Pb and Lu-Hf Isotopic Analyses of Early Cretaceous Oceanic Islands and Ophiolites, Tectonophysics., 655, 27-40, https://doi.org/10.1016/j. tecto.2015.04.019, 2015.

Faccenna, C., Speranza, F., Caracciolo, F.D., Mattei, M. and Oggiano, G.: Extensional tectonics on Sardinia (Italy): insights into the arc-back-arc transitional regime, Tectonophysics., 365, 213-232, https://doi.org/10.1016/S0040-1951(02)00287-1, 2002.

Fu, X. G., Wang, J., Wen, H. G., Song, C. Y., Wang, Z. W., Zeng, S. Q., Feng, X. L., Wei, H. Y.: A Toarcian Ocean Anoxic Event record from an open-ocean setting in the eastern Tethys: Implications for global climatic change and regional environmental perturbation, Sci china earth sci., 64, 1860-1872, https://doi.org/10.1007/s11430-020-9753-1, 2021.

Garcia-Lasanta, C., Oliva-Urcia, B., Roman-Berdiel, T., et al.: Evidence for the Permo-Triassic transtensional rifting in the Iberian Range (NE Spain) according to magnetic fabrics results, Tectonophysics., 651-652, 216-231, https://doi.org/10.1016/j.tecto.2015.03.023, 2015.

Grove, T. L., Till, C. B., Lev, E., et al.: Kinematic variables and water transport control the formation and location of arc volcanoes, Nature, 459, 694-697, https://doi.org/10.1038/nature08044, 2009.

Gurioli, L., Pareschi, M. T., Zanella, E., et al.: Interaction pyroclastic density currents with human settlements: Evidence from ancient Pompeii, Geology., 33, 441-444, https://doi.10.1130/g21294.1, 2005

Gvirtzman, Z., and Nur, A.: The formation of Mount Etna as the consequence of slab rollback, Nature., 401, 782-785, https://doi.org/10.1038/44555, 1999.

Guynn, J., Kapp, P., Pullen, A., Heizler, M., Gehrels, G., and Ding L.: Tibetan basement rocks near Amdo reveal "missing"Mesozoic tectonism along the Bangong suture, central Tibet, Geology., 34, 505-508, https://doi.org/10.1130/G22453.1, 2006.

Hermann, J., Rubatto, D., Korsakov, A., et al.: Multiple Zircon Growth During Fast Exhumation of Diamondiferous, Deeply Subducted Continental Crust (Kokchetav Massif, Kazakhstan), Contrib mineral petr., 141, 66-82, https://doi.org/10.1007/s004100000218, 2001.

Hrouda, F.: Magnetic a2001. nisotropy of rocks and its application in geology and geophysics, Geophysical Surveys., 5, 37-82, https://doi.org/10.1007/BF01450244, 1982.

Hrouda, F.: A technique for the measurement of thermal changes of magnetic susceptibility of weakly magnetic rocks by the CS-2 apparatus and KLY-2 Kappabridge, Geophys j int., 118, 604-612, https://doi.10.1111/j.1365-246X.1994.tb03987.x, 1994.

Hrouda, F.: Modelling relationship between bulk susceptibility and AMS in rocks consisting of two magnetic fractions represented by ferromagnetic and paramagnetic minerals-Implications for understanding magnetic fabrics in deformed rocks, J geol soc india., 75, 254-266, https://doi.10.1007/s12594-010-0013-0, 2010.

Hu, P. Y., Zhai, Q. C., Jahn, B. M., Wang, J., Li, C., et al.: Late Early Cretaceous magmatic rocks(118-113Ma) in the middle segment of the Bangong-Nujiang suture zone, Tibetan Plateau: Evidence of lithospheric delamination, Gondwana res., 44, 116-138, https://doi.org/10.1016/j.gr.2016.12.005, 2017.

Huang, T. T., Xu, J. F., Chen, J. L., et al.: Sedimentary record of Jurassic Northward subduction of the Bangong-Nujiang Ocean: Insights from detrital zircons, Int geol rev., 59, 166-184, https://doi.org/10.1080/00206814.2016.1218801, 2017.

Ishizuka, O., Tani, K., Reagan, M. K., et al.: Izu-Bonia-Mariana Forearc Crust as a Modern Ophiolite Analogue, Elements., 10, 115-120, 2014.

Jelinek, V.: Characterization of the magnetic fabric of rocks, Tectonophysics., 79, T63-T67, https://doi.org/10.1016/0040-1951(81)90110-4, 1981.

Kapp, P., Decelles, P. G., Gehrels, G. E., Heizler, M., and Ding L.: Geological records of the Lhasa-Qiangtang and Indo-Asian collisions in the Nima area of Central Tibet, Geological Society on America Bulletin., 119, 917-933, https://doi.org/10.1130/B26033.1, 2007.

Kneen, S.: The relationship between the magnetic and strain fabrics of some haematite-bearing Welsh slates, Earth planet sci lett., 31, 413-416, https://doi.org/10.1016/0012-821X(76)90123-0, 1976.

Larrasoana, J. C., Pueyo, E. L., and Pares, J. M.: An integrated AMS, structural, palaeo- and rock-magnetic study of Eocene marine marls from the Jaca-Pamplona basin (Pyrenees, N Spain): new insights into the timing of magnetic fabric acquisition in weakly deformed mudrocks. Geological Society, London, Special Publications., 238, 127-144, https://.doi.org/10.1144/GSL.SP.2004.238.01.10, 2004.

Li, F. Q., Tang, J. X., Zhang, J., Song, Y., Li, H. F., Lin, B. and Wang, N.: Discovery of Late Early Cretaceous diorite porphyrite from the Shamuluo Formation in the Gaize area, Tibet: Response to the northward subduction plate rollback event of Bangongco-Nujiang Tethys Ocean, Acta Petrological Sinica., 38, 185-208, https://doi.org/10.18654/1000-0569/2022.01.13, 2022.

Li, S., Ding, L., Guilmette, C., et al.: The Subduction-Accretion History of the Bangong-Nujiang Ocean: Constraints from Provenance and Geochronology of the Mesozoic Strata near Gaize, Central Tibet, Tectonophysics., 702, 42-60, https://doi.org/10.1016/j.tecto.2017.02.023, 2017.

Li, Z. Y., Ding, L., Lippert, P. C., et al.: Paleomagnetic constraints on the Mesozoic drift of the Lhasa terrane (Tibet) from Gondwana to Eurasia, Geology., 44, 727-730, https://doi.org/10.1130/G38030.1, 2016.

Li, Z. Y., Ding, L., Song, P. P., et al.: Paleomagnetic constraints on the paleolatitude of the Lhasa block during the Early Cretaceous: Implications for the onset of India-Asia collision and latitudinal shortening estimates across Tibet and stable Asia, Gondwana res., 41, 352-372, https://doi.org/10.1016/j.gr.2015.05.013, 2017.

Liu, D.L., Huang, Q. S., Fan, S. Q., Zhang, L. Y., et al.: Subduction of the Bangong-Nujiang Ocean: constraints from granites in the Bangong Co area, Tibet, Geol j., 49, 188-206, https://doi.org/10.1002/gj.2510, 2014.

Liu, Y. S., Hu, Z. C., Zong, K. Q., et al.: Reappraisement and Refinement of Zircon U-Pb Isotope and Trace Element Analyses by LA-ICP-MS, Chin sci b-chin., 55, 1535-1546, https://doi.org/10. 1007/ s11434-010-3052-4, 2010.

https://doi.org/10.5194/egusphere-2022-1214
Preprint. Discussion started: 9 January 2023

Lu, R. K., Zhang, G. W., Zhong, H. M., et al.: Characteristics of magnetic fabrics in western segment of the Altun fault belt and its tectonic significance, Chinese J. Geophys., 51, 752-761, https://doi.org/10.1002/cjg2.1244, 2008.

Luo, L., Jia, D., Li, H. B., et al.: Magnetic fabric investigation in the northwestern Sichuan Basin and its regional inference, Phys earth planet in., 173, 103-114, https://doi.10.1016/J. PEPI. 2008.11.004, 2009.

Ma, A. L., Hu, X. M., Kapp, P., et al.: The disappearance of the Late Jurassic Remnant Sea in the Southern Qiangtang Block (Shamuluo Formation, Najiangco Area): Implications for the Tectonic Uplift of Central Tibet, Palaeogeogr palaeocl., 506, 30-47, https://doi.org/10.1016/j. palaeo.2018.06.005, 2018.

Ma, Y., Yang, T., Bian, W., et al.: Paleomagnetic and geochronology results of latest Cretaceous lava flows from the Lhasa Terrane and their tectonic implications, J geophys res-sol ea., 122, 8786-8809, https://doi.org/10.1002/2107JB014743, 2017.

Metcalfe, I.: Gondwana dispersion and Asian accretion: Tectonic and palaeogeographic evolution of eastern Tethys, J Asian earth sci., 66, 1-33, https://doi.org/10.1016/j.jseaes.2012.12.020, 2013.

Pan, G. T., Wang, L. Q., Li, R. S., et al.: Tectonic evolution of the Qinghai-Tibet Plateau, J asian earth sci., 53, 3-14, https://doi.org/10.1016/j.jseaes.2011.12.018, 2012.

Pares, J. M., van der Pluijm, B. A., Dinares-Turell, J.: Evolution of magnetic fabrics during incipient deformation of mudrocks (Pyrenees, northern Spain), Tectonophysics., 307, 1-14, https://doi.10.1016/S0040-1951(99)00115-8, 1999.

Pares, J. M.: How deformed are weakly deformed mudrocks? Insights from magnetic anisotropy, Geological Society, London, Special Publications., 238, 191-203, https://doi.10.1144/gsl.so.2004.238.01.13, 2004.

Rathore, J. S.: Application of magnetic susceptibility anisotropy technique to the study of geological structures in the Armorican massif, France, Tectonophysics., 60, 207-216, https://doi.org/10.1016/0040-1951(79)90159-8, 1979.

Saint-Bezar, B., Herbert, R. L., Aubourg, C., et al.: Magnetic fabric and petrographic investigation of hematite-bearing sandstones within ram-related folds: examples from the South Atlas Front (Morocco), J struct geol., 24, 1507-1520, https://doi.10. 1016/S0191-8141(01)00140-7, 2002.

Scheepers, P. J. J., and Langereis, C. G.: Magnetic fabric of Pleistocene clays from the Tyrrhenian arc: A magnetic lineation induced in the final stage of the middle Pleistocene compressive event, Tectonics., 13, 1190-1200, https://doi.org/10.1029/94TC00221, 1994.

Schmidt, V., Gunther, D., and Hirt, A. M.: Magnetic anisotropy of calcite at room-temperature, Tectonophysics., 418, 63-73, https://doi.10.1016/j.tecto.2005.12.019, 2006.

Song, C. H., Zeng, Y. Y., Yan, M. D., Wu, S., et al.: Magnetostratigraphy of the middle-upper Jurassic sedimentary sequences at Yanshiping, Qiangtang Basin, China, Geophys j int., 206, 1847-1863, https://doi.org/10.1093/gji/ggw199, 2016.

Tarling, D., and Hrouda, F.: The magnetic anisotropy of rocks, London: Chapman and Hall., 1-189, 1993.

Wang, B. D., Wang, L. Q., Chung, S. L., et al.: Evolution of the Bangong-Nujiang

https://doi.org/10.5194/egusphere-2022-1214
Preprint. Discussion started: 9 January 2023

Tethyan ocean: insights from the geochronology and geochemistry of mafic rocks within ophiolites, Lithos., 245, 18-33, https://doi.org/10.1016/j.lithos.2015.07.016, 2016.

Wang, K., Jia, D., Luo, L., et al.: Magnetica fabric and structural deformation, Chines J. Geophys., 60, 1007-1026, https://doi.10.6038/cjg20170315, 2017.

Whattam, S. A., and Stern, R. J.: The "subduction initiation rule": a key for linking ophiolites, intra-oceanic forearcs, and subduction initiation, Contrib mineral petr., 162, 1031-1045, https://doi.org/10.1007/s00410-011-0638-z, 2011.

Wu, H., Li, C., Xu, M. J., et al.: Early Cretaceous Adakitic Magmatism in the Dachagou Area, Northern Lhasa Terrane, Tibet: Implications for Slab Roll-Back and Subsequent Slab Break-off of the Lithosphere of the Bangong-Nujiang Ocean, J asian earth sci., 97, 51-66, https://doi.org/10.1016/j.jseaes.2014.10.014, 2015.

Wu, H. N.: Magnetic fabric of rock and its application in analysis of rock deformation, Acta Petrol. Sin., 52, 2588-2594, 1988.

Wu, J. L., Liu, W., Yin, X. K., Lei, C. Y., and Wang, B.: Geochronology, Zircon Hf Isotope and Geochemistry of volcanic Rocks from Shamuluo Formation in Western Bangongco-Nujiang Suture Zone, North Tibet, Earth-sci rev., 46, 444-459, https://doi.org/10.3799/dqkx.2020.104, 2021.

Xie, G. G., Mo, X. X., Zhao, Z. D., et al.: Jurassic-Cretaceous sedimentation and evolution of ancient oceanic basic in Bangong Lake area, Tibet, Earth Science Frontiers., 16, 031-039, 2009.

Xu, Y. J., Du, Y. S., Cawood, P. A.,et al.: Detrital Zircon Record of Continental collison: Assembly of the Qilian Orogen, China, Sediment geol., 230, 35-45, https://doi.org/10.1016/j.sedgeo.2010.06.020, 2010.

Yin, A., and Harrison, T. M.: Geological evolution of the Himalayan-Tibetan Orogen, Annu rev earth pl sc., 28, 211-280, 2000.

Zeng, S. Q., Wang, J., Zeng, Y. H., et al.: Episodic volcanic eruption and arid climate during the Triassic-Jurassic transition in the Qiangtang Basin, eastern Tethys: A possible linkage with the end-Triassic biotic crises, J asian earth sci., 237, https://doi.org/10.1016/j.jseaes.2022.105345, 2022.

Zeng, Y. Y., Gao, L., and Zhao, W. Q.: Paleoclimate evolution and aridification mechanism of the eastern Tethys during the Callovian-Oxfordian: evidence from geochemical records of the Qiangtang Basin, Tibetan Plateau, Acta Geochimica., 40, 199-211, https://doi.org/10.1007/s11631-021-00458-2, 2021.

Zhu, D. C., Zhao, Z. D., Niu, Y. L., et al.: The Lhasa Terrane: record of a microcontinent and its histories of drift and growth, Earth planet sc lett., 301, 241-255, https://doi.org/10.1016/j.epsl.2010.11.005, 2011.

Zhu, D. C., Li, S. M., Cawood, P. A., Wang, Q., Zhao, Z. D., Liu, S. A., and Wang, L. Q.: Assembly of the Lhasa and Qiangtang terranes in central Tibet by divergent double subduction, Lithos., 245, 7-17, https://doi.org/10.1016/j.lithos.2015.06.023, 2016.

Zhou, Y. N., Cheng, X., Yu, L., et al.: Paleomagnetic study on the Triassic rocks from the Lhasa Terrane, Tibet, and its paleogeographic implications, J asian earth sci., 121, 108-119, https://doi.org/10.1016/j.jseaes.2016.02.006, 2016.